$O(\alpha_s)$ Monte Carlo approach to W+Higgs-boson associated production at hadron supercolliders

H. Baer, B. Bailey, and J. F. Owens
Department of Physics, Florida State University, Tallahassee, Florida 32306
(Received 29 October 1992; revised manuscript received 21 December 1992)

We calculate the $O(\alpha_s)$ corrections to the process $pp \to W^{\pm}HX \to l\nu\gamma\gamma X$ using a Monte Carlo approach. Complete spin correlations are included. We examine the size of QCD corrections before and after minimal cuts on the final state, for both the Superconducting Super Collider and the CERN Large Hadron Collider. By comparing the WH cross section to the single-W cross section, some uncertainties due to parton distributions may also be eliminated. Comparison of the theoretical cross section with an observed event rate may allow one to distinguish between the presence of a standard model or minimal supersymmetric model intermediate mass Higgs boson.

PACS numbers: 13.85.Qk, 12.38.Bx, 14.80.Er, 14.80.Gt

I. INTRODUCTION

One of the most important goals in particle physics is to understand the origin of electroweak symmetry breaking. In the standard model (SM), electroweak symmetry breaking takes place via the Higgs mechanism, for which one of the byproducts is the existence of a fundamental scalar particle, the Higgs boson [1]. Nonobservation of the SM Higgs boson (H) at the four CERN LEP experiments has resulted in a mass limit [2],

$$m_H > 57 \text{ GeV}.$$

Experiments at LEP 200 ought to be able to discover H provided $m_H \lesssim 90$ GeV [3]. Also, if $2M_Z \lesssim m_H \lesssim 800$ GeV, then at least the "gold-plated" $H \to ZZ \to 4l$ decay mode (where $l = e$ or μ) should be visible at Superconducting Super Collider (SSC) and/or CERN Large Hadron-Collider (LHC) experiments [1].

If the Higgs boson is in the so-called "intermediate-mass region," 90 GeV$\lesssim m_H \lesssim 2M_Z$, then it will not be observable at LEP 200, and its dominant decay mode into $b\bar{b}$ will be hopelessly mired beneath QCD backgrounds at hadron supercolliders. In this case, one must hope to search for rare decay modes of the Higgs boson, such as $H \to ZZ^*$ [4] or $H \to \gamma\gamma$ [5]. The former decay mode occurs at observable rates when H is at the upper range of intermediate Higgs-boson masses; the latter mode occurs at an observable rate throughout the intermediate mass region, but must be searched for against a large background from continuum photon pair production [6]. Detection of the inclusive process $pp \to H \to \gamma\gamma$ will require detectors with excellent $\gamma\gamma$ mass resolution [7].

The production of $H \to \gamma\gamma$ in association with a W boson has been proposed as an alternative to the above inclusive process. Here, one would search for $pp \to WH \to l\nu\gamma\gamma X$ [8]. Requiring the presence of a hard, isolated lepton in the event eliminates direct photon pair production as a background; one must consider instead the background $pp \to W\gamma\gamma X$. Signal and background for the associated production mechanism has been calculated in Ref. [8]. It was found that signal events are expected to occur at a cross section of ~ 1 fb (0.3 fb) at the SSC (LHC) for m_H in much of the intermediate mass region, which ought to yield an observable mass bump against the $W\gamma\gamma$ background if sufficiently high luminosity is attained. In addition, the signal can be augmented by a factor ~ 6 (~ 2) at the SSC (LHC) by including the $t\bar{t}H$ production process [9]. In this case, one would search for $t\bar{t}H \to bl\nu bqq'\gamma\gamma$ events, which will be complicated by additional hadronic activity in the central region.

To facilitate comparison between experiment and theory, the best possible estimates of the total signal cross section and background are needed. For instance, the leading-log (LL) QCD calculation of $pp \to WH$ has an intrinsic uncertainty depending upon the choice of factorization scale of up to about 50%. A next-to-leading-log (NLL) calculation of the $pp \to WH$ total cross section has been performed in Ref. [10], where it was shown that the scale uncertainty can be reduced to the few percent level. Of course, the QCD corrections are phase-space dependent, and also depend on the particular cuts placed upon an event sample. With this in mind, we have performed an independent calculation of the NLL corrections to $pp \to WH \to l\nu\gamma\gamma$ using a Monte Carlo approach. We include full spin correlations of the final-state decay products. Such an approach allows us to easily calculate total cross sections or any observable distribution at the NLL level. Furthermore, greater accuracy in the theoretical prediction of the observed $l\nu\gamma\gamma$ event rate can be obtained, since cuts at the parton level are easily incorporated into our Monte Carlo approach. The rest of this paper is organized as follows. In Sec. II, we describe in some detail our calculation, including the relevant formulae needed to set up a NLL Monte Carlo calculation of $pp \to WH \to l\nu\gamma\gamma$. In Sec. III, we present numerical results for the total signal cross section, before and after including a possible set of cuts and acceptances on final-state particles. We show that the NLL cross sections are indeed phase-space dependent. Further uncertainty can enter theoretical cross section estimates due to vari-

ations between sets of parton distributions. To reduce this uncertainty as well, we advocate examination of the ratio $\sigma(WH \to l\nu\gamma\gamma)/\sigma(W \to l\nu)$. Some of the additional parton distribution function uncertainty cancels out upon taking this ratio. In Sec. IV, we present some general conclusions, and discuss the possibility of distinguishing between a SM and minimal supersymmetric standard model (MSSM) Higgs boson based on a measured event rate.

II. CALCULATION

The Monte Carlo formalism for NLL calculations has been described in detail in Refs. [11–13] so the discussion here will be brief. The basic challenge is to design a program which retains the versatility inherent in a Monte Carlo approach while ensuring that all of the required cancellations of singularities still takes place. In order to discuss the technique for isolating the various singularities, let the four-vectors of the three-body and four-body subprocesses be labeled by $p_1 + p_2 \to p_3 + p_4 + p_5$ and $p_1 + p_2 \to p_3 + p_4 + p_5 + p_6$, respectively, and define the Lorentz scalars $s_{ij} = (p_i + p_j)^2$ and $t_{ij} = (p_i - p_j)^2$. This calculation contains infrared (IR) and collinear singularities but no ultraviolet singularities. Dimensional regularization is used to isolate the singularities. First, four-body phase space is partitioned into singular and finite regions by introducing soft and collinear cutoff parameters, δ_s and δ_c. The soft region of phase space is defined to be the region where the gluon energy in the subprocess rest frame becomes less than $\delta_s\sqrt{s}_{12}/2$. The collinear regions of phase space are defined to be those regions where any invariant (s_{ij} or t_{ij}) becomes smaller in magnitude than $\delta_c s_{12}$. Next, the squared four-body matrix elements are approximated in the singular regions; the soft gluon and leading-pole approximations are used in the soft and collinear regions, respectively. The resulting expressions are then integrated over the singular regions of phase space. At this stage the integrated expressions contain finite three-body contributions as well as singular pieces. The singularities from the soft region will cancel the virtual IR singularities while the singularities from the collinear region will be factorized into the parton distribution functions. The remainder of four-body phase space contains no singularities and the subprocesses can be evaluated in four dimensions.

The calculation now consists of two pieces—a set of three-body contributions and a set of four-body contributions. Each set consists of finite parts, all singularities having been cancelled or factorized. At this stage both pieces depend on the values chosen for the two theoretical cutoffs δ_s and δ_c so that each piece by itself has no intrinsic meaning. However, when the three- and four-body contributions are combined to form a suitably inclusive observable all dependence on the cutoffs cancels. The cutoffs merely serve to distinguish the regions where the phase space integrations are done by hand from those where they are done by numerical Monte Carlo methods. When the results are added together, the precise location of the boundary between the two regions is not relevant. The results reported below are stable to reasonable variations in the cutoffs, thus providing a check on the calculation.

To perform this calculation one needs the necessary matrix elements and corrections. The three-body cross section consists of a Born term, plus higher-order contributions. These higher-order terms may be found in Ref. [12], taking care to replace the misprinted first factor of π^2 by the correct factor of $\frac{2}{3}\pi^2$ in Eq. (A7). The labeling of four-momentum is as follows:

$$q(p_1) + \bar{q}'(p_2) \longrightarrow l(p_3) + \nu(p_4) + H(p_5).$$

The Born matrix element, summed and averaged over color and spin, is

$$\overline{\sum}|M_{\rm Born}|^2 = \left(\frac{64}{3\sqrt{2}}\right) \frac{M_W^8 G_F^3 t_{13} t_{24}}{|D_W(s_{12})|^2 |D_W(s_{34})|^2}, \tag{1}$$

where

$$|D_W(s)|^2 = (s - M_W^2)^2 + (M_W \Gamma_W)^2.$$

The four-body cross section consists of annihilation and Compton contributions. The labeling of four-momenta for the anihilation reaction is

$$q(p_1) + \bar{q}'(p_2) \longrightarrow l(p_3) + \nu(p_4) + H(p_5) + g(p_6).$$

The annihilation matrix element, summed and averaged over color and spin, is

$$\overline{\sum}|M_A|^2 = \left(\frac{512}{3\sqrt{2}}\right) \frac{\alpha_s(Q^2)\pi C_F M_W^8 G_F^3}{|D_W(s_{345})|^2 |D_W(s_{34})|^2} \left[\frac{s_{36}t_{24} - t_{13}t_{14} + t_{13}t_{24}}{t_{16}} + \frac{s_{46}t_{13} + t_{13}t_{24} - t_{23}t_{24}}{t_{26}} + \frac{s_{12}(s_{36}t_{24} + s_{46}t_{13} + 2t_{13}t_{24})}{t_{16}t_{26}} \right], \tag{2}$$

where $s_{345} = (p_3 + p_4 + p_5)^2$ and $C_F = \frac{4}{3}$. The Compton matrix element may be obtained by crossing and multiplication by the appropriate color factor. Combining these matrix elements with the formalism of Ref. [12] allows for straightforward evaluation of the LL and NLL cross sections. The decay of $H \to \gamma\gamma$ can be easily included, since it doesn't alter the above matrix elements. We calculate the $H \to \gamma\gamma$ decay in the H center-of-mass frame

and boost to the hadron-hadron center-of-mass frame. We then multiply the total cross section by the $H \to \gamma\gamma$ branching fraction to obtain the final cross section.

III. RESULTS

For the results reported below the following were used: Harriman-Martin-Roberts-Stirling set B (HMRS-B) parton distributions [14], a two-loop expression for the running coupling $\alpha_s(Q^2)$, $M_W = 80.22$ GeV and $\Gamma_W = 2.12$ GeV.

One of the sources of uncertainty in our calculation comes from the choice of squared factorization scale M^2. Usually the scale is chosen such that $Q^2 = M^2$, where Q is some large energy scale relevant to the problem. For most of our results, we take $Q^2 = M^2_{WH}$; however, other choices are also logical possibilities, such as $Q^2 = nM^2_{WH}$, where $n \sim 1$. In an all-orders calculation, all large scales are equivalent and the cross section is insensitive to a particular choice of scale. However, in a fixed-order calculation this dependence remains. In Figure 1(a) we show the Q^2 variation of the cross section $\sigma(pp \to W^{\pm}H \to l\nu\gamma\gamma)$, where l is summed over e and μ. We adopt $m_H = 120$ GeV and $\sqrt{s} = 40$ TeV for the SSC. We see (as in Ref. [10]) that the LL cross section can vary by up to $\sim 50\%$ over the range of n shown. The NLL cross section is much less dependent on variations of scale, and only changes by $\sim 7\%$.

If we apply a minimal set of cuts on final-state p_T and pseudorapidity η [e.g., $p_T(l,\gamma) > 20$ GeV and $|\eta(l,\gamma)| < 2.5$], then we obtain Fig. 1(b). Both the LL and NLL cross sections are reduced, but by unequal amounts. In particular, the point at which the net QCD corrections to the LL result are zero has moved from $n \sim 2$ to $n \sim 4$. Comparison of Figs. 1(a) and 1(b) shows that the slope of the $q\bar{q}$ correction is nearly unchanged, while the slope of the qg correction is reduced $\sim 50\%$. The cuts induce this change by excluding the lower-x_T regions of phase space where the gluon luminosity is large, thereby reducing the negative qg contribution. This phenomenon occurs for the LHC energy of $\sqrt{s} = 16$ TeV as well.

TABLE I. Cross sections (fb) at the SSC without cuts.

m_H	$\sigma_{\rm LL}$	$\sigma_{\rm NLL}$	$\sigma_{\rm NLL}/\sigma_{\rm LL}$	$10^8\sigma^{WH}_{\rm NLL}/\sigma^{W}_{\rm NLL}$
80	1.94	2.07	1.07	5.06
100	1.89	2.02	1.07	4.94
120	1.69	1.79	1.06	4.37
140	1.02	1.08	1.06	2.64

In Figs. 2(a) and 2(b) we plot the distributions in $p_T(\gamma)$ and $p_T(l)$ before any cuts are applied, for the same parameters as above, except taking $n = 1$. The plots show LL (dashed curves) and NLL (solid curves) predictions. The $p_T(\gamma)$ distribution has twice the area since both final state photons have been included. The regions of large $p_T(\gamma)$ and $p_T(l)$ are enhanced at NLL level, which can be attributed to the nonzero p_T of the W^* ($W^* \to WH$). Hence, we expect that after p_T cuts have been applied, the ratio of $\sigma_{\rm NLL}/\sigma_{\rm LL}$ increases. Overall, the NLL final-state particle p_T distributions are in accord with the LL results; in particular, QCD effects apparently do not lead to an observable difference in these final-state distributions.

In Tables I–IV, the production cross sections are presented for SSC and LHC energies, using $n = 1$. Tables I and II give the production cross sections at the SSC, without and with cuts respectively, for a range of Higgs-boson masses. Tables III and IV give similar information for the LHC. Table I shows that the QCD corrections, without cuts, are of order $\sim 10\%$ or less (from column 4). This can be understood from the Q^2 variation curve shown in Fig. 1(a). Without cuts and with $Q^2 = M^2_{WH}$, the positive $q\bar{q}$ corrections are nearly balanced by the negative qg corrections. In Table II, after cuts, we see that the QCD corrections have risen to typically $\sim 10\%$. More severe cuts can affect cross-section measurements even further. For instance, vetoing jet activity with $p_T(\text{jet}) > 25$ GeV can reduce the NLL cross section by a factor of 2; such a cut, of course, would not affect the LL estimate.

Another source of uncertainty in calculating cross sec-

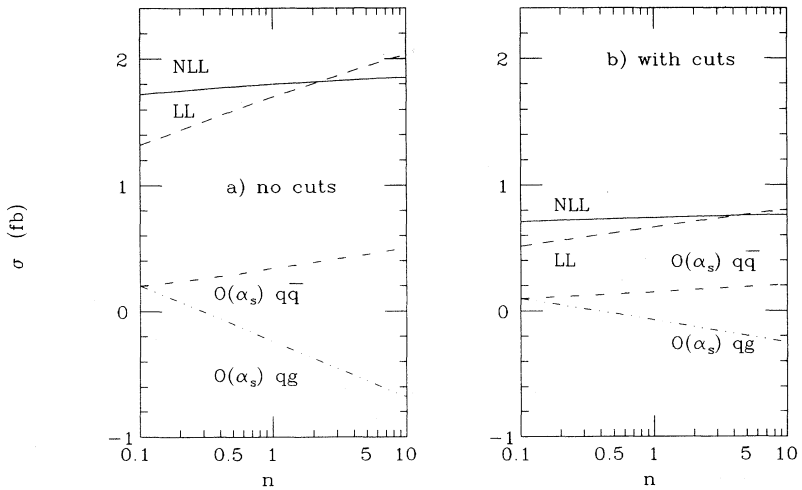

FIG. 1. (a) Q^2 variation of the cross section at the SSC without cuts, where we have taken $Q^2 = nM^2_{WH}$. (b) Q^2 variation of the cross section at the SSC with $p_T(\gamma, l) > 20$ GeV, $|\eta(\gamma, l)| < 2.5$. The results are summed over $W^{\pm}$ and $l = e$ or μ. We have taken $m_H = 120$ GeV.

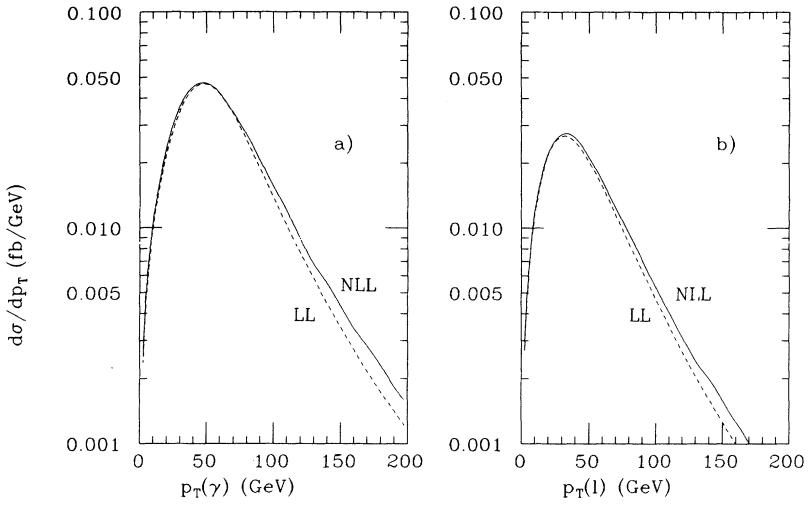

FIG. 2. (a) Transverse momentum distribution of the γ's without cuts for m_H = 120 GeV, at SSC energy. (b) Transverse momentum distribution of the lepton without cuts.

tions comes from parton distribution functions. At supercollider energies the variation in total cross section due to using different sets of parton distribution functions may be as large as 30%. This variation may be reduced by calculating a reference process cross section and forming the ratio of the two processes, thus canceling out some of the dependence on the parton distribution functions. For WH associated production a likely reference process is ordinary single W production. To this end, the cross sections for WH and W production plus decay were compared at the NLL level for two different sets of parton distribution functions. The two sets of parton distribution functions used were HMRS-B and Martin-Roberts-Stirling set D0 (MRS-D0) [15], which have been fit to different data sets at low x. The value for the ratio of the cross sections is

$$\frac{\sigma^{WH}_{\rm NLL}(\text{MRS-D0})}{\sigma^{WH}_{\rm NLL}(\text{HMRS-B})} \sim 1.30,$$

whereas the ratio of referenced ratios is

$$\frac{\sigma^{WH}_{\rm NLL}(\text{MRS-D0})}{\sigma^{W}_{\rm NLL}(\text{MRS-D0})} \Big/ \frac{\sigma^{WH}_{\rm NLL}(\text{HMRS-B})}{\sigma^{W}_{\rm NLL}(\text{HMRS-B})} \sim 0.93.$$

The referenced ratio is less sensitive to parton distribution function differences and thus one may further reduce theoretical uncertainty. The ratio $\sigma^{WH}_{\rm NLL}/\sigma^{W}_{\rm NLL}$, with and without cuts, can be found in Tables I–IV, where $\sigma^{WH}_{\rm NLL}$ refers to $\sigma(pp \to W^{\pm} \to l\nu)$, with $l = e$ or μ.

IV. CONCLUSIONS

We have performed a NLL Monte Carlo calculation for $pp \to WH \to l\nu\gamma\gamma$, including complete spin correlations for final state particles. Incorporating mild experimental cuts on final state particles can cause deviations of a few percent in the ratio $\sigma_{\rm NLL}/\sigma_{\rm LL}$—an unobservable effect. Incorporation of more severe cuts can of course affect this ratio much more.

In a real experimental situation, various cuts such as lepton and photon isolation will have to be imposed to eliminate backgrounds from processes such as $b\bar{b}\gamma\gamma$ where $b \to cl\nu$, and from processes such as $W\gamma$+jet production, where the jet radiates a hard photon. Then, the bulk of $l\nu\gamma\gamma$ events would come from $t\bar{t}H$ production, with a smaller contribution from WH production, while major backgrounds will be from processes such as $W\gamma\gamma$ and $t\bar{t}\gamma\gamma$. The latter backgrounds yield a continuum in $m(\gamma\gamma)$, while the signal yields, of course, a sharp peak [16]. At the SSC, the rate for $l\nu\gamma\gamma$ events from $t\bar{t}H$ production actually occurs at $\sim 5-6$ times the rate from WH production, while at LHC energy, the ratio is ~ 2. The $t\bar{t}H$ cross section at LL level at either of these colliders probably has an uncertainty of a factor of ~ 2. Hence it is desirable to know the QCD corrections to the $t\bar{t}H$ cross section as well as for the background processes. However, given a sufficiently large event sample, it may be possible to separate the candidate Higgs events of WH origin, as opposed to those of $t\bar{t}H$ origin. This might be accomplished, for instance, by requiring no jet

TABLE II. Cross sections (fb) at the SSC with $p_T > 20$ GeV, $|\eta| < 2.5$.

m_H	$\sigma_{\rm LL}$	$\sigma_{\rm NLL}$	$\sigma_{\rm NLL}/\sigma_{\rm LL}$	$10^8\sigma^{WH}_{\rm NLL}/\sigma^{W}_{\rm NLL}$
80	0.59	0.65	1.10	4.65
100	0.68	0.74	1.09	5.29
120	0.67	0.73	1.09	5.23
140	0.43	0.47	1.09	3.36

TABLE III. Cross sections (fb) at the LHC without cuts.

m_H	$\sigma_{\rm LL}$	$\sigma_{\rm NLL}$	$\sigma_{\rm NLL}/\sigma_{\rm LL}$	$10^8\sigma^{WH}_{\rm NLL}/\sigma^{W}_{\rm NLL}$
80	0.78	0.84	1.08	3.52
100	0.75	0.81	1.08	3.40
120	0.65	0.71	1.09	2.98
140	0.38	0.42	1.10	1.76

TABLE IV. Cross sections (fb) at the LHC with $p_T > 20$ GeV, $|\eta| < 2.5$.

m_H	$\sigma_{\rm LL}$	$\sigma_{\rm NLL}$	$\sigma_{\rm NLL}/\sigma_{\rm LL}$	$10^8\sigma^{WH}_{NLL}/\sigma^{W}_{NLL}$
80	0.30	0.33	1.10	3.76
100	0.34	0.38	1.12	4.33
120	0.33	0.37	1.12	4.22
140	0.21	0.23	1.10	2.62

activity above a nominal p_T value in the central region, or by tagging displaced b-decay vertices. In this case, a direct comparison of the WH event rate with theoretical expectations may be possible.

It is interesting to ask then if a discrimination may be made between the presence of a SM Higgs boson, and the presence of a Higgs boson from physics beyond the SM. For instance, in the minimal supersymmetric model, there exist [1] two neutral scalar Higgs bosons, a light and heavy scalar (H_l and H_h), which can give rise to $l\nu\gamma\gamma$ events. Both of these can have branching ratios into $\gamma\gamma$ that approach those of the SM Higgs boson [17]. It has recently been shown that there exist regions of the MSSM parameter space where the $l\gamma\gamma$ signature should be observable at hadron supercolliders [17]. The $l\gamma\gamma$ events from the MSSM would be exactly the same as SM events in terms of distributions, with the only possible difference (aside from the presence of other classes of events indicating SUSY) being in the total event rate.

The couplings of H_l [H_h] to WW differ from those of the SM Higgs boson by a factor of $\sin(\alpha+\beta)$ [$\cos(\alpha+\beta)$], where $\tan\beta = \frac{v}{v'}$, the ratio of Higgs field vacuum expectation values VEV's, and α is a mixing angle between the scalar Higgs states [18]. These factors cause a reduction in the WH_l and WH_h production cross sections relative to the corresponding standard model rate. In addition, the MSSM Higgs-boson branching ratios into $\gamma\gamma$ can frequently be smaller than the SM value by large amounts—factors of 2–5 are not uncommon [17,18]. This occurs mainly due to the presence of superpartner contributions to the $H \to \gamma\gamma$ loop graphs. Such differences can contribute to detectable differences in the total event rate. For instance, for a SM Higgs boson, obtaining an integrated luminosity $L \sim$ few $\times 10^2$ fb^{-1} at the SSC could yield about 80 $WH \to l\gamma\gamma$ events, with a 3σ uncertainty of ~ 30 events. In this case, differences in the $l\nu\gamma\gamma$ event rates of a factor of $2-3$ could be detected.

Note added. After completion of this work, we received a preprint by J. Ohnemus and W. Stirling, Ref. [19], where very similar work is reported. We have checked that the results presented here are consistent with those of Ref. [19].

ACKNOWLEDGMENTS

We thank U. Baur, C. Kao, and X. Tata for useful discussions. This research was supported in part by the U.S. Department of Energy under Contract No. DE-FG05-87ER40319.

[1] J. Gunion, H. Haber, G. Kane, and S. Dawson, *The Higgs Hunter's Guide* (Addison-Wesley, Redwood City, CA, 1990).

[2] S. L. Wu, in *The Vancouver Meeting—Particles and Fields '91*, Proceedings of the Joint Meeting of the Division of Particles and Fields of the American Physical Society and Particle Physics Division of the Canadian Association of Physicists, Vancouver, 1991, edited by D. Axen, D. Brymen, and M. Comyn (World Scientific, Singapore, 1992), Vol. 1.

[3] H. Georgi, G. Glashow, M. Machacek, and D. Nanopoulos, Phys. Rev. Lett. **40**, 692 (1978); J. Gunion and L. Roszkowski, in *Research Directions for the Decade*, Proceedings of the 1990 Summer Study on High Energy Physics, Snowmass, Colorado, edited by E. Berger (World Scientific, Singapore, 1991); V. Barger and K. Whisnant, Phys. Rev. D **43**, 1443 (1991).

[4] W. Y. Keung and W. Marciano, Phys. Rev. D **30**, 248 (1984).

[5] J. Gunion, G. Kane, and J. Wudka, Nucl. Phys. **B299**, 231 (1988).

[6] H. Baer and J. F. Owens, Phys. Lett. B **205**, 377 (1988).

[7] R. Zhu, Caltech Report No. CALT-68-1777, 1992 (unpublished).

[8] R. Kleiss, Z. Kunszt, and J. Stirling, Phys. Lett. B **253**, 269 (1991).

[9] W. Marciano and F. Paige, Phys. Rev. Lett. **66**, 2433 (1991); J. Gunion, Phys. Lett. B **261**, 510 (1991).

[10] T. Han and S. Willenbrock, Phys. Lett. B **273**, 167 (1990).

[11] H. Baer, J. Ohnemus, and J. F. Owens, Phys. Rev. D **40**, 2844 (1989); **42**, 61 (1990); Phys. Lett. B **234**, 127 (1990).

[12] H. Baer and M. H. Reno, Phys. Rev. D **43**, 2892 (1991).

[13] B. Bailey, J. Ohnemus, and J. F. Owens, Phys. Rev. D **46**, 2018 (1992).

[14] P. N. Harriman, A. D. Martin, R. G. Roberts, and W. J. Stirling, Phys. Rev. D **42**, 798 (1990).

[15] A. D. Martin, R. G. Roberts, and W. J. Stirling, University of Durham Report No. DPT-92-48, 1992 (unpublished).

[16] Z. Kunszt, Z. Trocsanyi, and W. J. Stirling, Phys. Lett. B **271**, 247 (1991).

[17] J. Gunion and L. Orr, Phys. Rev. D **46**, 2052 (1992); Z. Kunszt and F. Zwirner, Nucl. Phys. **B385**, 3 (1992); V. Barger *et al.*, Phys. Rev. D **46**, 4914 (1992).

[18] H. Baer, M. Bisset, C. Kao, and X. Tata, Phys. Rev. D **46**, 1067 (1992); H. Baer, M. Bisset, D. Dicus, C. Kao, and X. Tata, Phys. Rev. D **47**, 1062 (1992).

[19] J. Ohnemus and W. J. Stirling, preceding paper, Phys. Rev. D **47**, 2722 (1993).